

**UNCERTAINTY IN ESTIMATING
TISSUE MOTION FROM ULTRASONIC IMAGES**

BY

ERIC CHUNG-JAY CHEN

B.S., University of Illinois, 1990

THESIS

Submitted in partial fulfillment of the requirements
for the degree of Master of Science in Electrical Engineering
in the Graduate College of the
University of Illinois at Urbana-Champaign, 1992

Urbana, Illinois

UNIVERSITY OF ILLINOIS AT URBANA-CHAMPAIGN

THE GRADUATE COLLEGE

MAY 1992

WE HEREBY RECOMMEND THAT THE THESIS BY
ERIC CHUNG-JAY CHEN

UNCERTAINTY IN ESTIMATING TISSUE MOTION
ENTITLED
FROM ULTRASONIC IMAGES

BE ACCEPTED IN PARTIAL FULFILLMENT OF THE REQUIREMENTS FOR
MASTER OF SCIENCE
THE DEGREE OF

W. O'Brien

Director of Thesis Research

W. K. Jenkins

N. Narayana Rao

Head of Department

Committee on Final Examination†

Chairperson

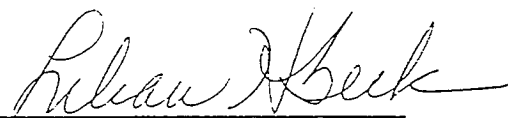
† Required for doctor's degree but not for master's.

UNIVERSITY OF ILLINOIS AT URBANA-CHAMPAIGN
GRADUATE COLLEGE DEPARTMENTAL FORMAT APPROVAL

THIS IS TO CERTIFY THAT THE FORMAT AND QUALITY OF PRESENTATION OF THE THESIS
SUBMITTED BY ERIC CHUNG-JAY CHEN AS ONE OF THE
REQUIREMENTS FOR THE DEGREE OF MASTER OF SCIENCE
ARE ACCEPTABLE TO THE DEPARTMENT OF ELECTRICAL AND COMPUTER ENGINEERING
Full Name of Department, Division or Unit

27 April 1992

Date of Approval



Departmental Representative

ABSTRACT

There has been recent interest in the utility of tissue motion analysis as a tool for sonographic tissue characterization. An important step in this process is the estimation of soft tissue motion from speckle motion in ultrasonic B-mode images. Because there is an imperfect correspondence between speckle motion and tissue motion, there is an associated uncertainty in quantitative estimates of tissue motion derived from speckle images. In this thesis, the variation of this uncertainty is studied as a function of tissue displacement, tissue type, and size of region of interest.

ACKNOWLEDGEMENTS

My thanks go to my advisors Professor William D. O'Brien, Jr., and Professor W. Kenneth Jenkins for all of their enthusiasm, encouragement and guidance. I would also like to thank my parents Wai-Fah and Lily and my younger brothers Arnold and Brian for their patience, understanding and moral support. Lastly, my sincere gratitude goes to Ilmar Hein, Jerome Chen and Ignatius Setiadi for their expertise and opinions. Tissue specimens were supplied through the courtesy of Professor Jan Novakofski of the Meat Sciences Laboratory in the Department of Animal Sciences and are gratefully acknowledged. Ultrasonic images of VX2 carcinoma in rabbit tissue and of human fetal lung tissue were supplied through Professor Ron Adler from the Department of Radiology, School of Medicine at the University of Michigan and his contributions are also gratefully acknowledged. This work was supported in part by NIH grant 5 T32 CA 09067.

TABLE OF CONTENTS

	Page
1. MOTIVATION AND BACKGROUND.....	1
1.1 Introduction	1
2. THEORETICAL MODEL.....	3
2.1 Estimation of Tissue Motion via Time-Domain Correlation	3
2.2 Limitations of the Time-Domain Correlation Technique	4
2.3 Interpretation of Normalized Correlation Coefficient.....	5
3. EXPERIMENTAL METHODS	7
3.1 Estimation of Calibrated Motion.....	7
3.1.1 Acquisition of image sequences	7
3.1.2 Estimation of interframe motion	10
3.1.3 Search region	12
3.2 Validation of the Time-Domain Correlation Technique.....	14
3.3 System Noise.....	15
3.3.1 Ambient noise	15
3.3.2 Resolution	16
3.4 Uncertainty and Precision of Tissue Motion Estimates	17
3.4.1 Computation of relative uncertainty	17
3.4.2 Computation of precision	18

4. RESULTS	21
4.1 Validation of Interframe Motion Estimation	21
4.2 Uncertainty of Motion Estimates	28
4.2.1 Porcine liver, porcine muscle and sponge	28
4.2.2 Variation of region of interest size	28
4.3 Precision of Motion Estimates	33
4.3.1 Porcine liver, porcine muscle and sponge	33
4.3.2 Variation of region of interest size	33
5. DISCUSSION	37
5.1 Interframe Motion of Samples	37
5.2 Dependence of Uncertainty on Tissue Type, ROI Size	38
and Actual Sample Displacement	
5.3 Dependence of Precision on Tissue Type, ROI Size	39
and Actual Sample Displacement	
6. CONCLUSIONS	40
REFERENCES	42

1. MOTIVATION AND BACKGROUND

1.1 Introduction

In diagnostic ultrasound the viscoelastic response of soft tissue has been used to characterize its physiological state [1-5]. Quantitative estimates of tissue compressibility, elasticity, lesion mobility and other viscoelastic properties of tissue are largely based on the accurate estimation of tissue displacements [6,7]. In evaluating tissue motion, quantitative estimates of viscoelastic tissue parameters are often compared with normal ranges [8]. Thus, it is essential to know the uncertainty associated with estimates of these parameters. The question we address in this study is how well speckle motion in ultrasonic images corresponds to actual tissue motion.

Preliminary studies have shown that there is a general inverse relation between the correspondence of speckle motion to tissue motion and applied deformation [9,10]. In this study, one of the goals is to quantify the limitations of the speckle tracking representation of tissue motion. The results of this thesis show how the imperfect correlation between speckle motion and tissue motion

affects the uncertainty in quantitative estimates of soft tissue motion. In addition, we will see how the uncertainty in motion estimates varies as a function of displacement, tissue type and size of region of interest. The results may help quantify the uncertainty associated with estimates of tissue strain and elasticity in tissue undergoing external deformation or graded compression.

2. THEORETICAL MODEL

2.1 Estimation of Tissue Motion via Time-Domain Correlation

An image can be represented by a two-dimensional array. In this case, each location in the array contains the intensity of a pixel in the image. (An image can also be viewed as a one-dimensional array if the rows of the two-dimensional array are concatenated to form a line). To estimate interframe motion between a pair of images represented by arrays A and B, the following time-domain correlation technique has been used. A rectangular region of interest (ROI) X is selected from image A. The ROI can be considered a subarray of A. A template region Y, with the same dimensions as X, is moved over all possible locations in image B. At each position a normalized correlation coefficient between X (the ROI in image A) and Y (the template in image B) is computed. A normalized correlation coefficient for discrete time functions can be computed using Equation (1) [11-14]:

$$\rho_{xy} = \frac{\sum_{i=0}^M \sum_{j=0}^N (x_{i,j} - \bar{x})(y_{i+k,j+l} - \bar{y})}{\sqrt{\sum_{i=0}^M (x_{i,j} - \bar{x})^2 \sum_{j=0}^N (y_{i+k,j+l} - \bar{y})^2}} \quad (1)$$

Here $x_{i,j}$ represents the pixel intensity inside of the ROI at coordinates (i,j) (i=0, j=0 is the origin, or bottom left corner of the rectangular ROI), $y_{i+k,j+l}$ represents the pixel intensity at position (i+k,j+l) in image B, (k,l) specify the coordinates of the origin of the template in the image B, and \bar{x} and \bar{y} denote the average pixel values in the ROI and in the template. Using this technique, the new position of the origin of the ROI X is assumed to be the position (k,l) in image B that produces the peak correlation coefficient.

2.2 Limitations of the Time-Domain Correlation Technique

The time-domain correlation technique presumes that the tissue in an ROI translates en-bloc, meaning that every pixel in the ROI is translated *by the same amount* in the axial and lateral directions. This technique *does not* account for rotations or deformations (expansion or compression) of tissue and these are critical limitations. Despite this fact, the time-domain correlation technique does provide a rough estimate of tissue motion. Because the normalized correlation coefficient is a measure of similarity (or linear relatedness), the time-domain

correlation technique does account for *uniform distortions* of intensity. If the pixel intensity x_{ij} of *every* pixel in an ROI X is distorted by an equivalent noise intensity z , the performance of the technique is not degraded. That is, the displacement of the ROI can still be tracked exactly ($\rho_{xy} = 1.0$). This is because the distorted ROI remains linearly related to the original ROI. Optical flow techniques exist that allow for off-line estimation of rotational and deformational components of motion [15]. However, one of the major advantages of the time-domain correlation technique is in its comparative computational efficiency. This technique has been implemented for measurement of blood flow and tissue motion in *real time* [16-17]. This makes the technique especially valuable for clinical application on-line.

2.3 Interpretation of Normalized Correlation Coefficient

The normalized correlation coefficient provides a measure of how linearly related two functions (or images) are. The normalization factor in the denominator of Equation (1) forces the correlation coefficient to take on values between -1.0 and 1.0. If two images X and Y are linearly related by $Y = cX$, where c is a constant, then the correlation coefficient for these images is ± 1.0 . (The relation $Y = cX$ means that every pixel in the image Y is a scaled version of its corresponding pixel in the image X).

A correlation coefficient of $\rho_{xy} = 1.0$ denotes exact similarity (but does not necessarily mean the images are identical). Consider two images with pixels identically distributed about two different means. These images are clearly not identical but are exactly similar and will produce a unitary correlation. A correlation coefficient $\rho_{xy} = -1.0$ represents an image inversion. For this case, pixel values x_{ij} in the image X are distributed a distance $|x_{ij} - \bar{x}|$ above or below \bar{x} . The corresponding pixels y_{ij} in the image Y are spaced by the same distance from \bar{y} but are in the opposite direction according to the relation

$$(x_{ij} - \bar{x}) = - (y_{ij} - \bar{y}) \quad (2)$$

Thus the image Y is identical to the image X, but is distributed and flipped about its mean \bar{y} . In other words, Y is the mirror image of X. Negative correlation coefficients are generally not useful in measuring similarity. In this sense, any positive correlation represents a greater similarity than any negative correlation.

3. EXPERIMENTAL METHODS

3.1 Estimation of Calibrated Motion

3.1.1 Acquisition of image sequences

Sections of porcine longissimus muscle and porcine liver were obtained from the Meat Sciences Laboratory, in the Department of Animal Sciences, at the University of Illinois. The porcine samples were obtained within 24 hours of death. The porcine liver and muscle were vacuum sealed. All measurements were made at room temperature (72 degrees F).

Ultrasonic images of rabbit tissue containing a VX2 carcinoma and human fetal lung tissue were obtained on standard VHS videotape from the Department of Radiology, School of Medicine at the University of Michigan. These images were used to help validate the time-domain correlation technique which is described in Section 3.2.

Samples of porcine liver, porcine muscle and woolen sea sponge were placed in a water tank and secured on top of sound absorbing (SOAB) slabs. Ultrasonic B-mode sector scans were obtained using a 5 MHz ATL transducer and an ATL MK 500 Ultrasonic Imager (Fig. 1). The ATL transducer was attached to the robotic arm of a Daedal motorized positioning system. The scanning plane of the transducer was aligned with one of the Daedal positioning axes by focusing on a thin fiberglass rod of radius 0.5 mm. The rod was submerged at a depth of 5.0 cm, the focal distance of the transducer. At this distance the beamwidth of the transducer is minimal and this allows for the tightest possible focusing.

In this study only en-bloc translations of samples were considered. That is, the time-domain correlation technique was used to estimate the incremental displacements of a selected ROI presuming that the dimensions of the ROI do not change. This accounts for translational motion of an ROI, but not for deformations in shape. The effects of shape deformations and vibrational motion have been reserved for future study. For porcine liver, porcine muscle and sponge, axial translations between 1.0 mm to 10.0 mm were executed using using a Daedal motorized positioning system, which has a precision of $\pm 1.0 \mu\text{m}$ for axial and lateral motions. Translations were executed in 1.0 mm increments.

After each 1.0 mm translation, an ultrasonic B-mode scan was digitized and saved using a Targa 16 frame grabbing system and a Compaq 386 computer.

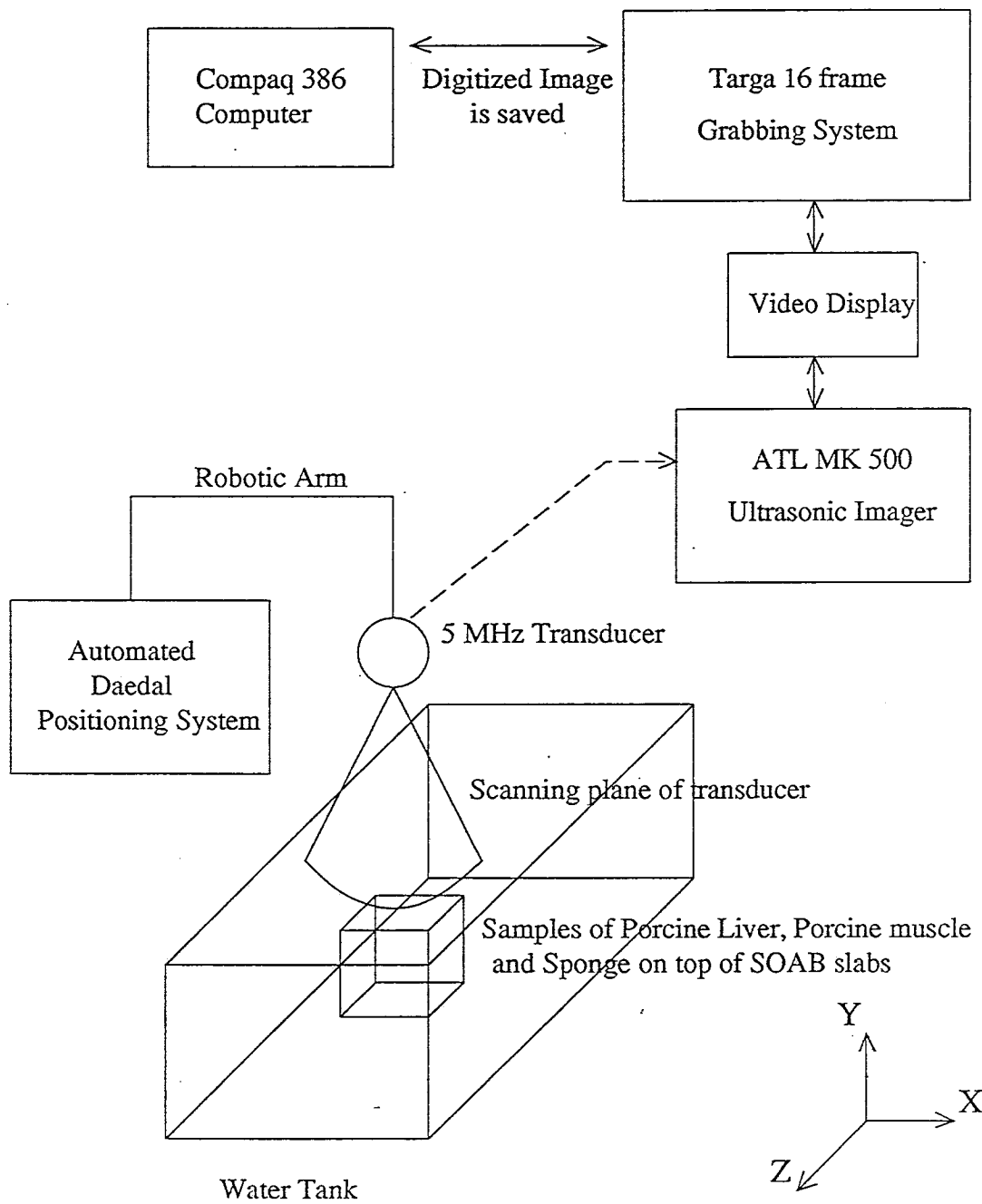


Fig. 1. Experimental Setup

Digitized image sequences were acquired for the porcine liver, porcine muscle and sponge samples. Motion was computed by estimating interframe motion (motion of samples between adjacent frames) and net motion (motion of samples between noncontiguous frames).

3.1.2 Estimation of interframe motion

To estimate interframe motion, a rectangular ROI was selected from the first frame of each sequence. The position and thus motion of the ROI was tracked through the image sequence in the following progressive manner. The motion of the ROI was tracked from its known starting position (i_1, j_1) in frame 1 to a position (i_2, j_2) in frame 2 using the time-domain correlation technique. Position (i_z, j_z) denotes the coordinates of the origin (bottom left corner) of the ROI in frame z . The ROI was then tracked from position (i_2, j_2) in frame 2 to (i_3, j_3) in frame 3 and so on (Fig. 2). This procedure was continued until the ROI was tracked to its final position (i_N, j_N) in frame N .

Using this technique, the position of the ROI is then known for each frame in the sequence. The net sample displacement can then be estimated between any two frames q and r in the sequence. As will be shown in Section 4.1, this turns out to be much more accurate than directly correlating two frames q and r , in estimating the net sample displacement between noncontiguous frames.

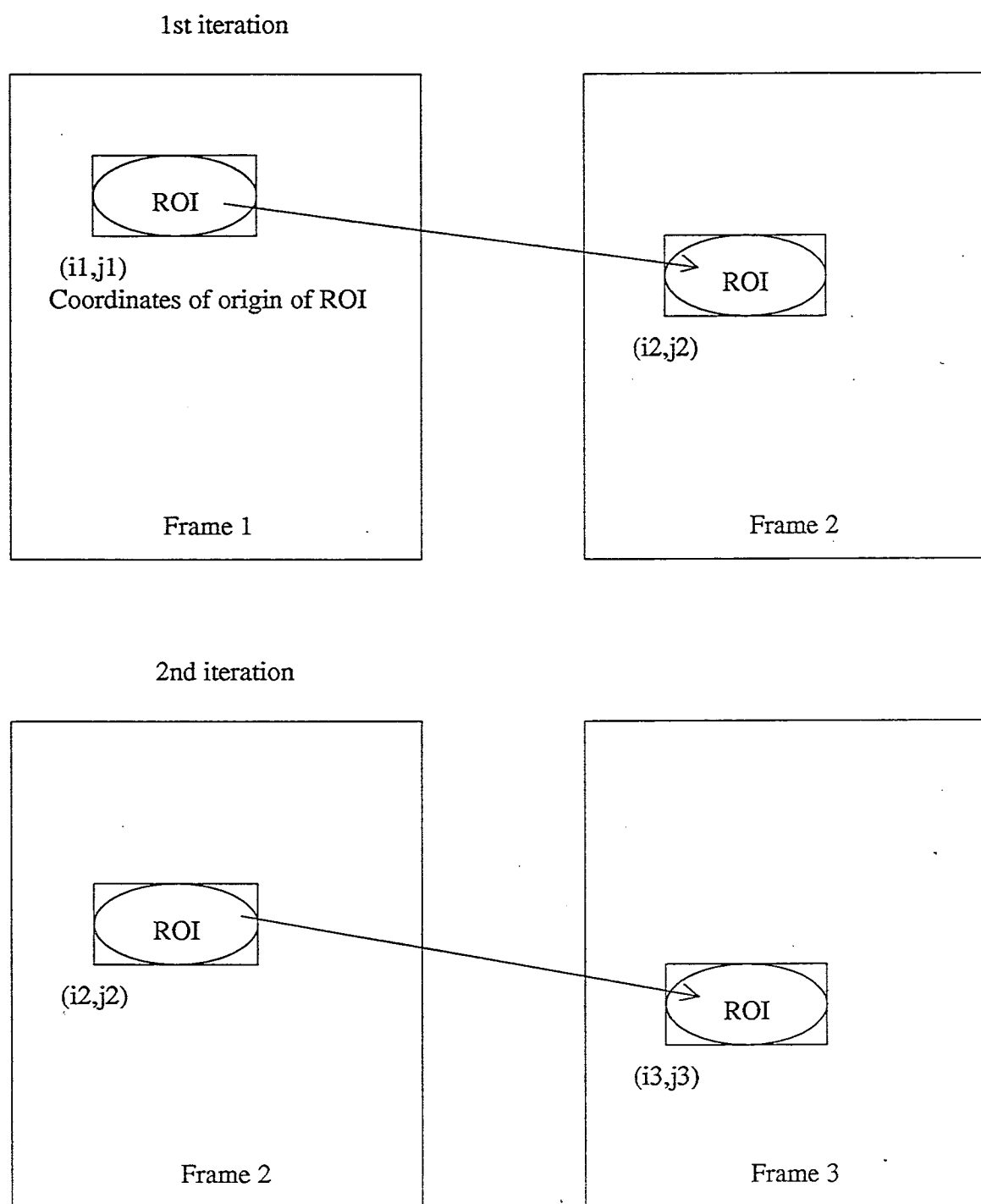


Fig. 2. Tracking the interframe motion of an ROI

3.1.3 Search region

For each frame to frame correlation, a search area was specified. A search area containing the entire image could have been specified, but a floating (moving) search area was used. Correlation-based searches sometimes detect false areas in an image which produce high correlation with specular reflectors, but are actually artifacts. To filter out some of these artifacts, it was assumed that if the elapsed time between frames was small, no section of tissue could translate more than a distance of M mm (or pixels). Translations were executed in increments of 1.0 mm, which corresponds to $M \approx 5$ pixels. The floating search area for a specular reflector or ROI in frame i consisted of the position and dimensions of the ROI in frame $i-1$, padded by $M=10$ pixels (or roughly 2.0 mm) in all directions (Fig. 3). This prevented searches in regions of an image which contained known artifacts.

The time-domain correlation algorithm was implemented by programs written in C language and run on Sun Sparc 330 and Sun Sparc 2 workstations. As a preliminary step, each sequence of images was first converted from standard RGB (Red-Green-Blue) color format to a 32 level grey scale format with a desired weighting function. In this case, the primary colors, red, green and blue were weighted equally. In RGB format, each pixel is represented by some percentage of each of these colors. That is, each pixel in an RGB image has a red intensity,

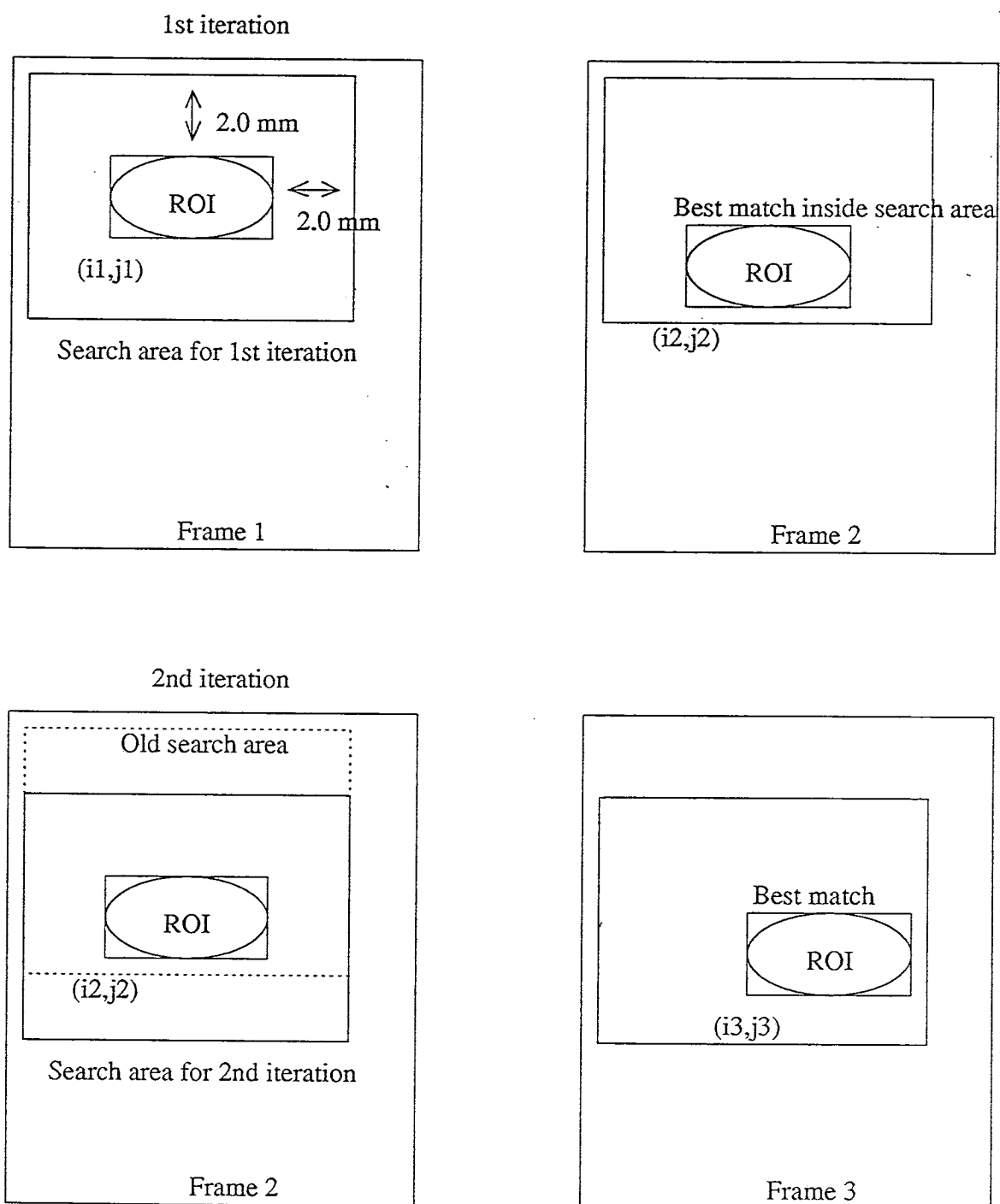


Fig. 3. Floating search region

green intensity and a blue intensity. To convert the RGB images to grey scale, these intensities were simply summed and averaged. Under this uniform weighting scheme, each of the primary colors is presumed to contribute an equal amount of brightness to the image. The converted images were then correlated in the progressive manner described above and the intermediate and final correlation coefficients and positions were saved.

3.2 Validation of the Time-Domain Correlation Technique

To validate the time-domain correlation technique, ultrasonic images of VX2 rabbit carcinoma, human fetal lung tissue, porcine liver, porcine muscle and woolen sea sponge tissue were digitized and saved. Rectangular ROIs with dimensions ranging from 5.0 mm by 5.0 mm to 40.0 mm by 40.0 mm were selected from images of each of the above tissues. A copy of each image was first generated. Each image was then correlated with itself. Rectangular regions were selected for convenience. More general geometries could be selected with appropriate modifications to software. In each case, the ROI was exactly tracked with a correlation coefficient of 1.0 and no change in position. This was exactly what was expected since frame 2 was a copy of frame 1 in each case and the ROI did not move.

Next, the time-domain correlation technique was used to track lesion areas in all of the above tissues and the results corresponded very well with those for visual comparison (lesion areas were tracked visually and when the time-domain correlation estimates of lesion motion were overlayed they appeared to fall on the centroids of the lesion areas). In addition, the time-domain correlation algorithms were used to exactly track the motion of a sequence of simple computer-generated images with correlation coefficients of 1.0. To help validate the progressive tracking software algorithms, the ROIs were tracked through a sequence of scans of the rabbit, fetal lung and porcine tissues in both the forward and reverse directions. (In the reverse direction the ROI was tracked from the end of the sequence back to the original frame.) For each sequence ROIs were tracked from a position (x_1, y_1) in frame 1 to a position (x_N, y_N) in frame N. The ROIs were then tracked in the reverse direction from position (x_N, y_N) in frame N to position (x_1, y_1) in frame 1 as expected. The results helped to verify that the progressive tracking software algorithms were implemented correctly.

3.3 System Noise

3.3.1 Ambient noise

To obtain a measure of the ambient noise in the system, the motion of a stationary ROI was tracked through a contiguous sequence of B-mode images. This

was done for 3 ROIs of different areas in porcine liver tissue and repeated for both porcine muscle tissue and sponge. In the absence of noise, the peak displacement of the ROI should be zero with a corresponding correlation coefficient of 1.0. In every case the actual peak displacement was found to be 0.0 mm for all samples. The mean correlation between consecutive images of stationary ROIs in all samples was 0.9960.

3.3.2 Resolution

The image resolution defines the smallest unit of motion. The resolution for tracking is 1 pixel length in the axial and lateral directions. Using 1 cm display markers on ultrasonic B-mode scans and the speed of sound in liver, muscle and water, a pixel to millimeter conversion ratio was computed for each tissue type. The finite resolution of B-mode scans (there are a finite number of pixels in each ultrasonic B-mode image) contributes to the uncertainty in estimates of tissue motion.

3.4 Uncertainty and Precision of Tissue Motion Estimates

3.4.1 Computation of relative uncertainty

The uncertainty in estimates of tissue motion for a given displacement were computed according to the relations:

$$displacement = \sqrt{|x_i - \hat{x}|^2 + |y_i - \hat{y}|^2} \quad (3)$$

$$uncertainty = \sqrt{|x_{i+1} - \hat{x}|^2 + |y_{i+1} - \hat{y}|^2} \quad (4)$$

$$relative\ uncertainty = 100 \left| \frac{uncertainty}{displacement} \right| \quad (5)$$

Here, (x_i, y_i) represents the initial position of the origin of an ROI, (\hat{x}, \hat{y}) represents the actual (known) position of the origin of an ROI after a translation is executed, and (x_{i+1}, y_{i+1}) represents the tracked position of the origin of an ROI after a translation is executed.

The uncertainty for a motion estimate is defined as the geometric distance between the actual final position of the ROI and the tracked final position of the ROI. It is a measure of the total error in the time-domain correlation technique due to noise and resolution. For each motion estimate, the uncertainty of that estimate represents a range of values around the estimate, in which the true value

may lie. In this case the true value is the known or actual tissue displacement. More specifically, for a given time-domain correlation estimate of a tissue displacement, the known tissue displacement should either be equal to the time-domain correlation estimate, or should fall within the range of uncertainty for that estimate.

Geometrically, the range of uncertainty for a motion estimate can be visualized as a circle centered about the estimate (Fig. 4). In general, as will be shown, as the known displacement increases, the range uncertainty for motion estimates increases. This can be visualized as larger and larger circular regions of uncertainty centered about the motion estimate. The relative uncertainty represents the uncertainty in an estimate of a tissue displacement normalized with respect to the actual displacement.

3.4.2 Computation of precision

For an actual displacement d , the precision of tissue motion estimates is defined by

$$p_d = \frac{\sigma_d}{\mu_d} \quad (6)$$

In Equation (6), μ_d and σ_d represent the mean and standard deviations of estimates of tissue displacements. The precision is a measure of the

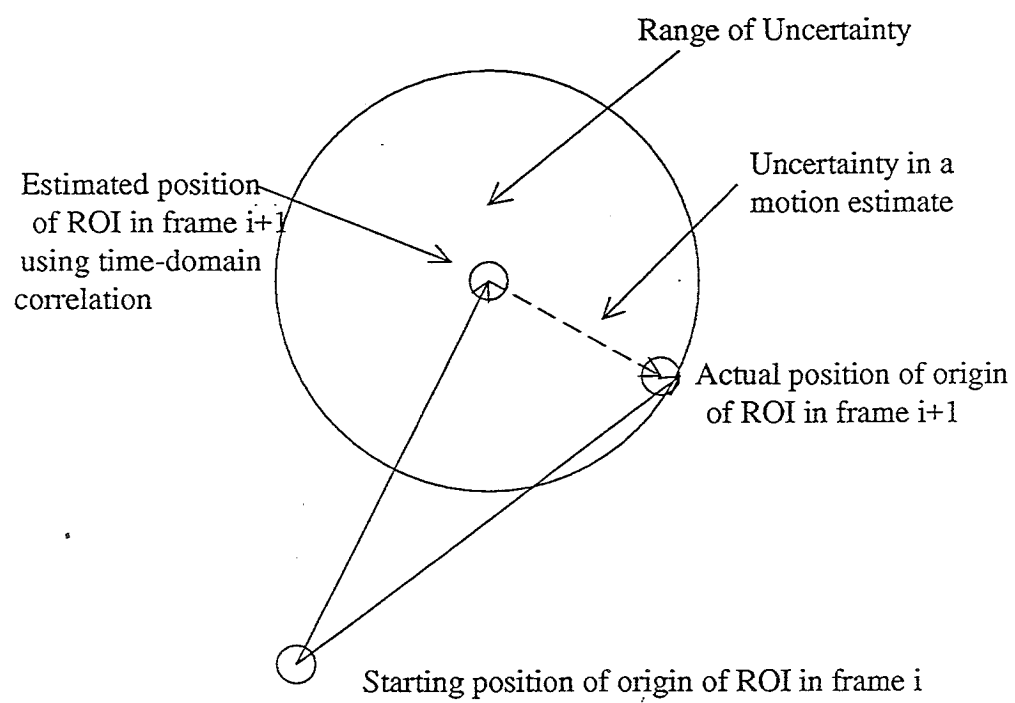


Fig. 4. Uncertainty for a known displacement

reproducibility of the time-domain correlation technique. It represents the normalized variance between estimates of tissue displacement.

4. RESULTS

4.1 Validation of Interframe Motion Estimation

To help validate the estimation of interframe motion discussed in Section 3.1.2, tissue displacements and sponge displacements were estimated by applying the time-domain correlation technique in two ways. First, motion between noncontiguous frames was estimated by tracking the motion of samples through intermediate frames. Second, motion between noncontiguous frames was estimated by directly correlating the noncontiguous frames. The uncertainty in time-domain correlation estimates of tissue displacement and sponge displacement is compared for these two methods in Figs. 5a-5c. Motion estimates, found by directly correlating noncontiguous frames, produced relative uncertainties exceeding 50% within 3.0 mm. Motion estimates, based on tracking motion in intermediate frames, produced approximately constant relative uncertainties on the order of 20% (Figs. 6a-6c).

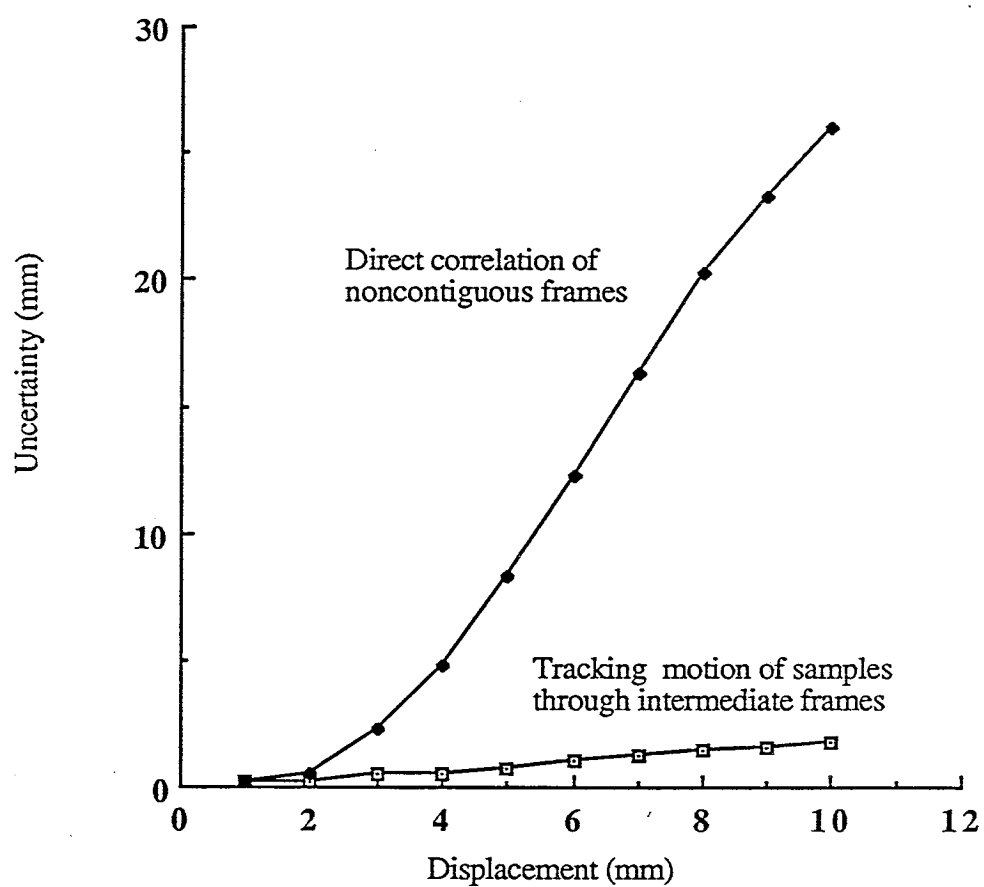


Fig. 5a. Uncertainty in axial motion estimates, sponge

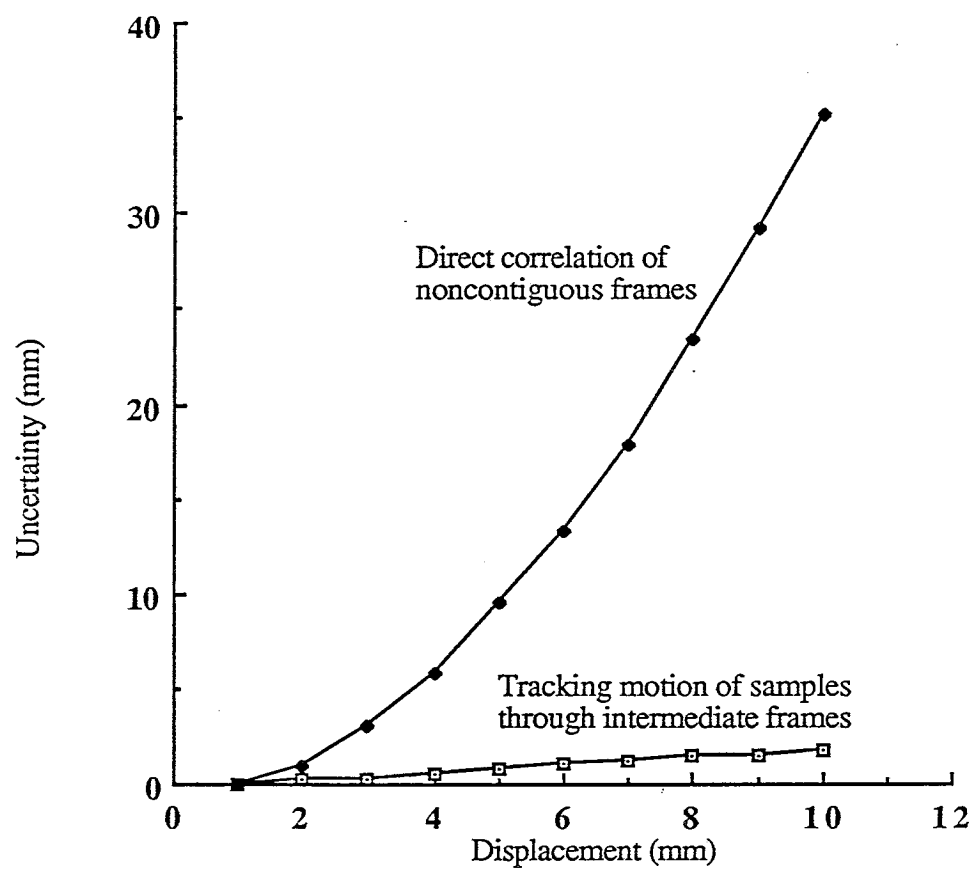


Fig. 5b. Uncertainty in axial motion estimates, liver

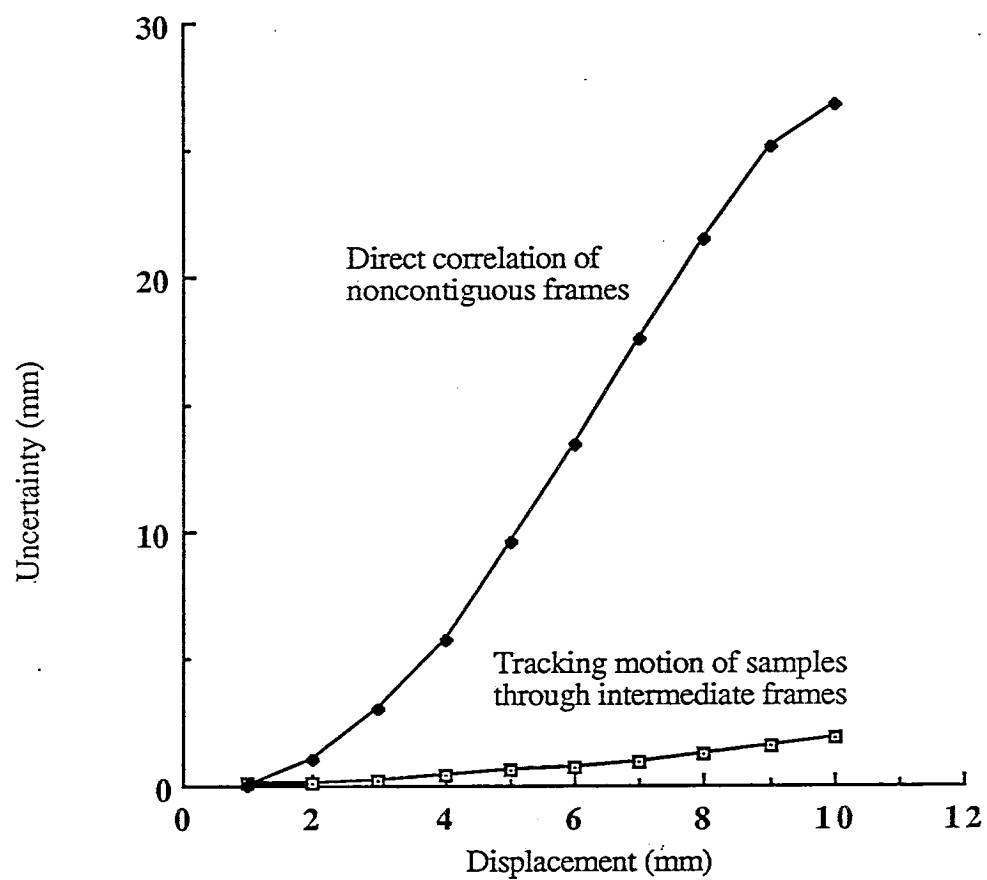


Fig. 5c. Uncertainty in axial motion estimates, muscle

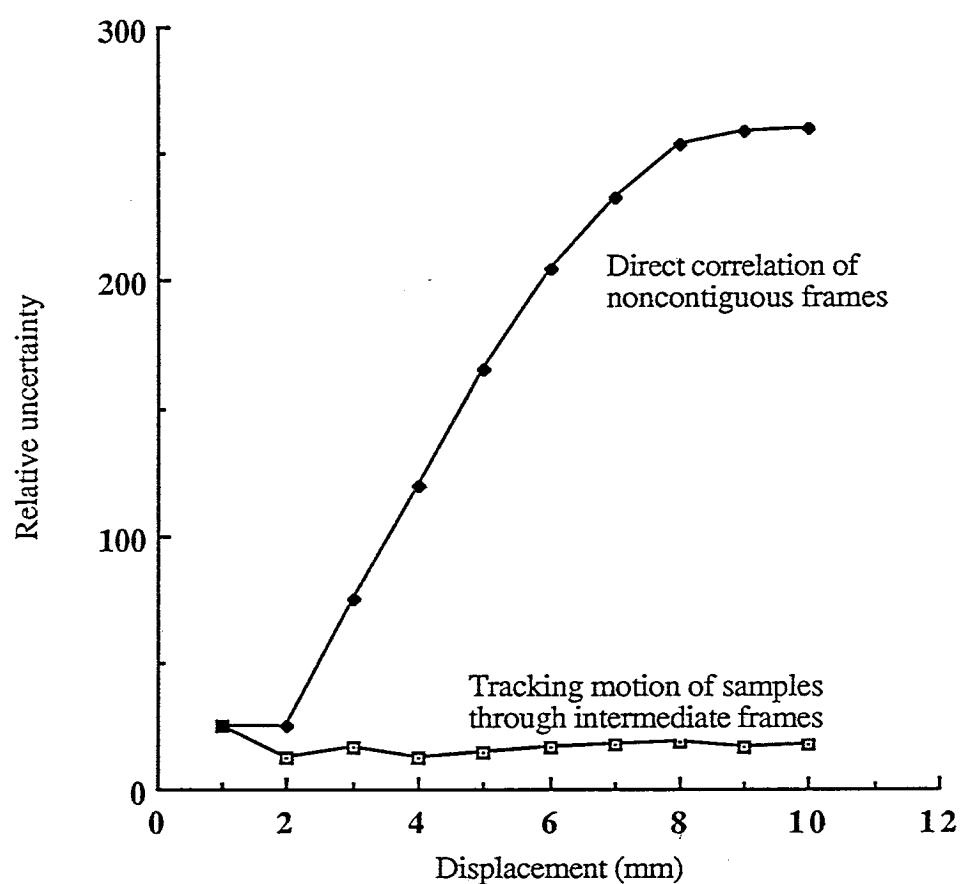


Fig. 6a. Relative uncertainty in axial motion estimates, sponge

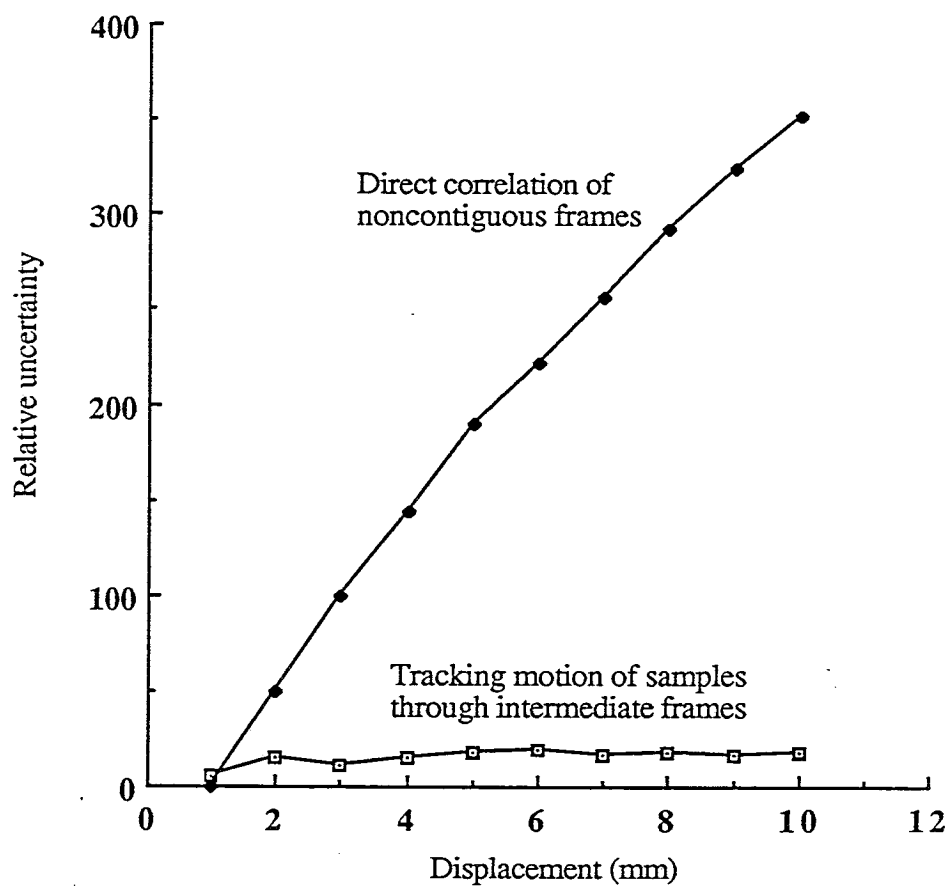


Fig. 6b. Relative uncertainty in axial motion estimates, liver

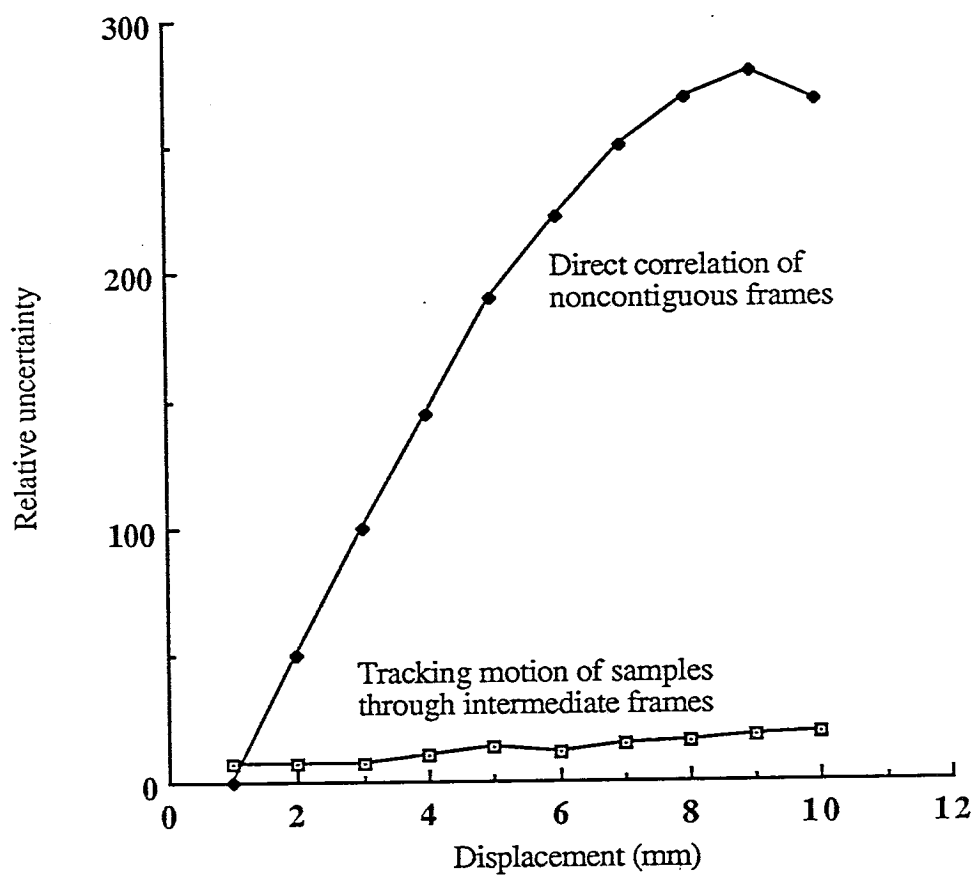


Fig. 6c. Relative uncertainty in axial motion estimates, muscle

4.2 Uncertainty of Motion Estimates

4.2.1 Porcine liver, porcine muscle and sponge

The uncertainty in motion estimates increases linearly as a function of actual sample displacement. This trend is illustrated in Fig. 7 for liver tissue, muscle tissue and sponge. Muscle tissue contains the greatest amount of internal structure [18]. As a result, ultrasonic B-mode scans of muscle tissue display greater texture than more homogeneous tissues [19] (in this case liver tissue or sponge). Thus, it is not surprising that motion estimates in muscle exhibit the smallest uncertainties. Motion estimates in all three samples produce relative uncertainties on the order of 20% (Fig. 8). This equates to an uncertainty of about 0.2 mm per mm for actual sample displacements less than 10.0 mm.

4.2.2 Variation of region of interest size

For liver tissue, muscle tissue and sponge the uncertainty in motion estimates increases for smaller and smaller regions of interest. In Figs. 9a and 9b the uncertainty in motion estimates is shown for ROIs with dimensions of 15.0 mm by 15.0 mm, 20.0 mm by 20.0 mm and 30.0 mm by 20.0 mm, in liver and muscle tissues. This corresponds to areas of 4900, 10,000 and 15,000 square millimeters respectively. The ROIs were selected so that they were all concentric. That is,

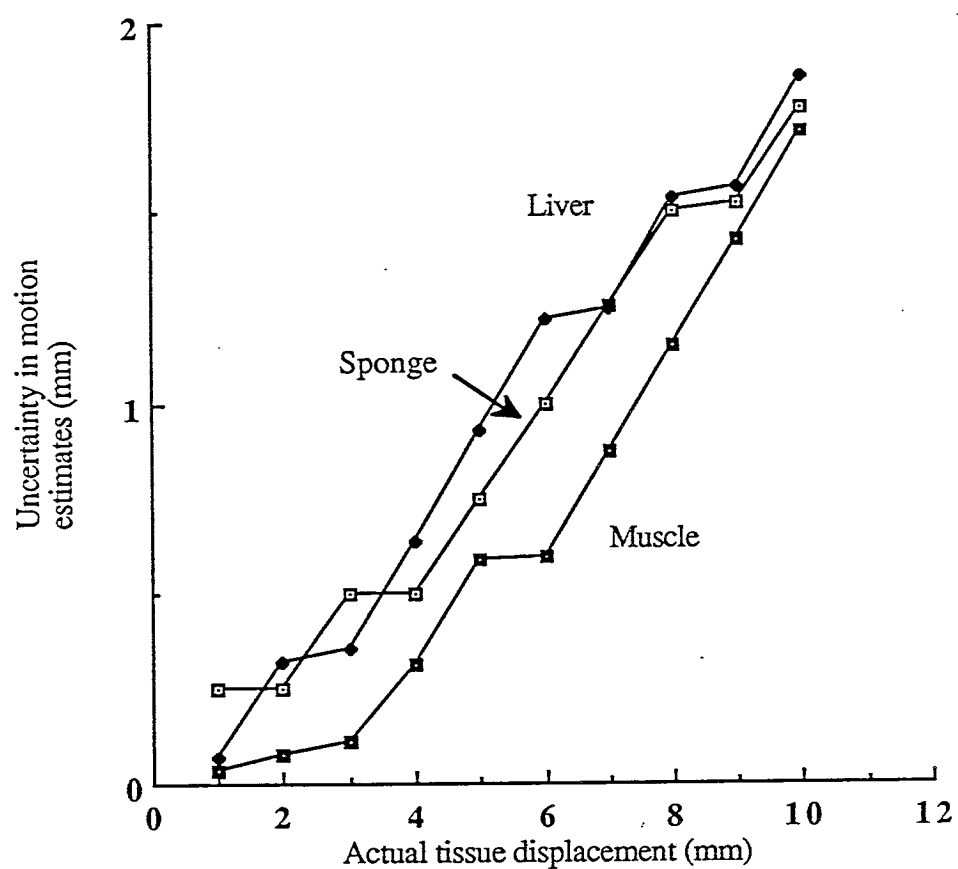


Fig. 7. Uncertainty in motion estimates for liver, muscle and sponge

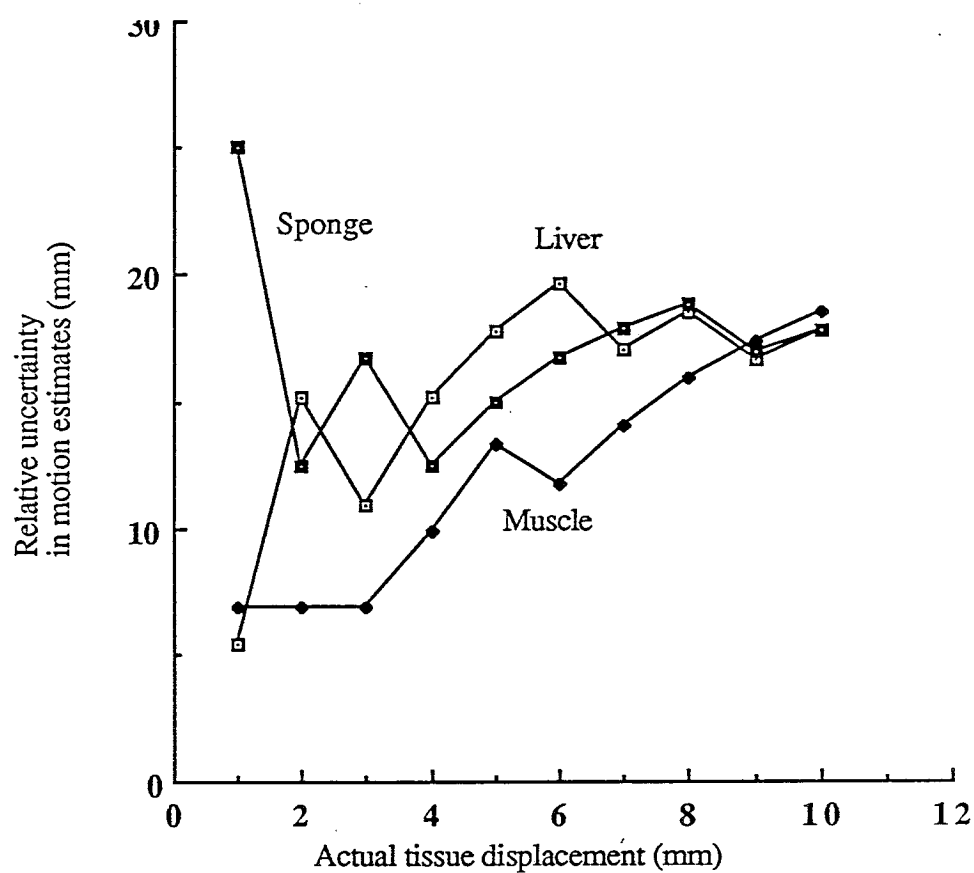


Fig. 8. Relative uncertainty in motion estimates in porcine liver, porcine muscle and sponge

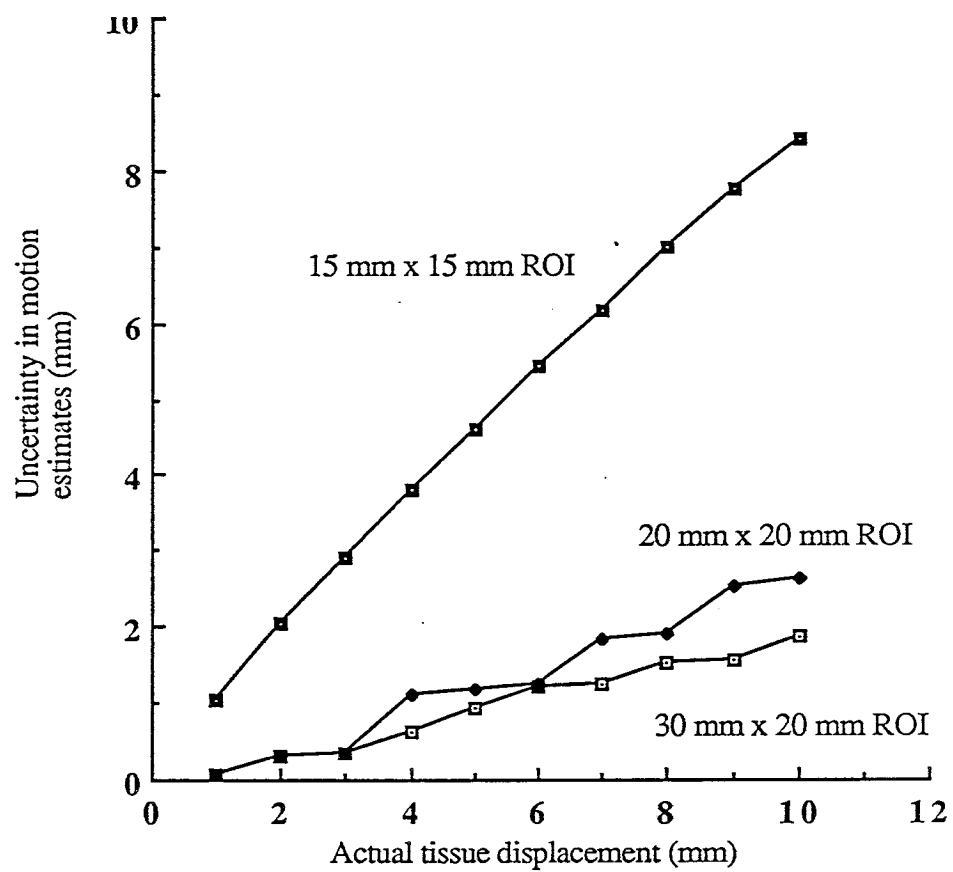


Fig. 9a. Uncertainty in motion estimates for three ROI sizes, liver

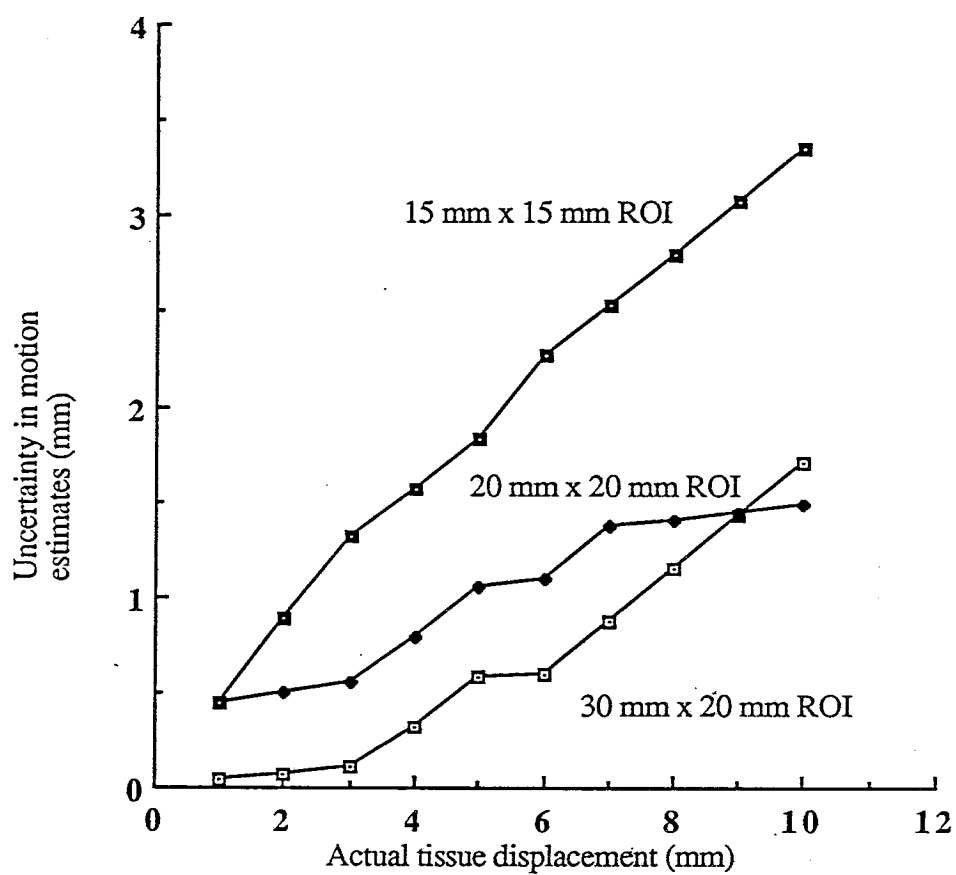


Fig. 9b. Uncertainty in motion estimates for three ROI sizes, muscle

the centroids of the ROIs are all at the same coordinates to ensure that roughly the same section of tissue is tracked.

4.3 Precision of Motion Estimates

4.3.1 Porcine liver, porcine muscle and sponge

The precision of motion estimates in liver tissue was found to be less than 0.07 for known sample displacements of less than 10.0 mm. This equates to deviations between motion estimates of at most 7% relative to mean motion estimates. The precision of motion estimates was found to be no worse than 2.1% for muscle tissue and 3.2% for sponge. Again, since muscle tissue contains the greatest amount of internal structure, it is not surprising that motion estimates in muscle tissue exhibit the highest precision.

4.3.2 Variation of region of interest size

The precision of motion estimates was computed for ROIs with dimensions of 15.0 mm by 15.0 mm, 20.0 mm by 20.0 mm and 30.0 mm by 20.0 mm, in liver tissue, muscle tissue and sponge. This corresponds to areas of 4900, 10,000 and 15,000 square millimeters. For all samples, the precision of motion estimates deteriorated as ROIs with smaller dimensions were selected (Figs. 10a-10c).

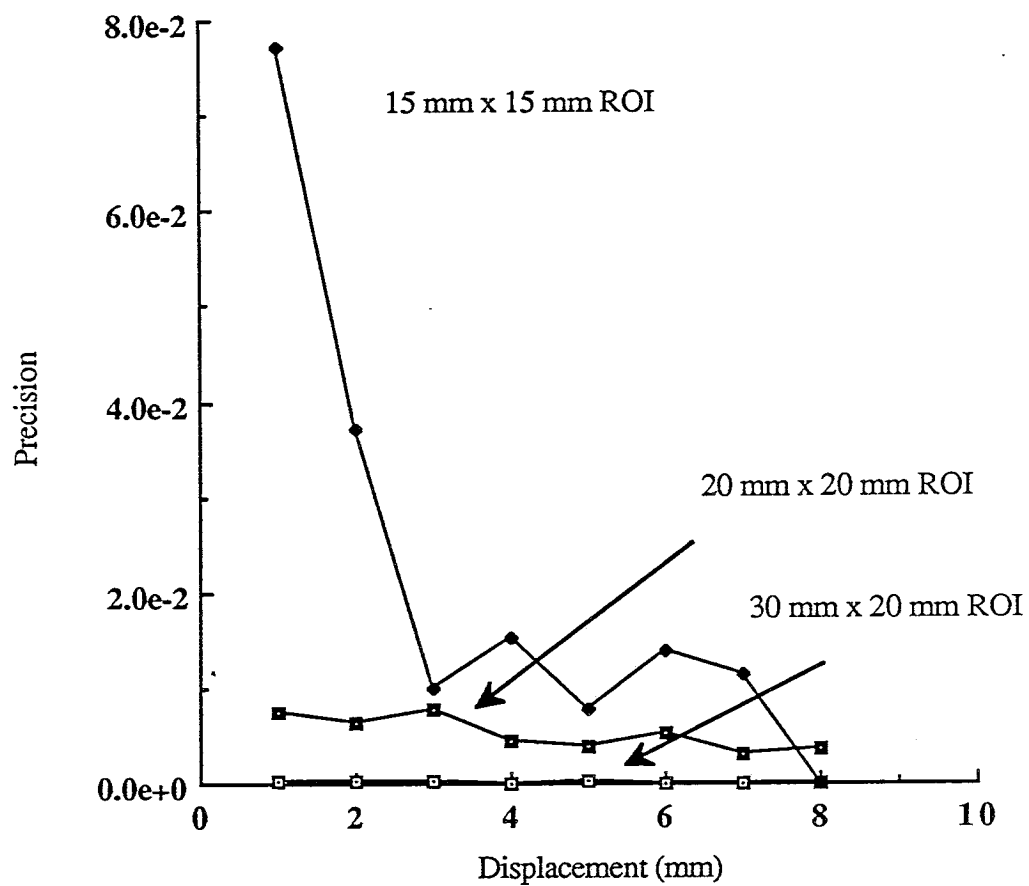


Fig. 10a. Variation of precision with size of region of interest, liver

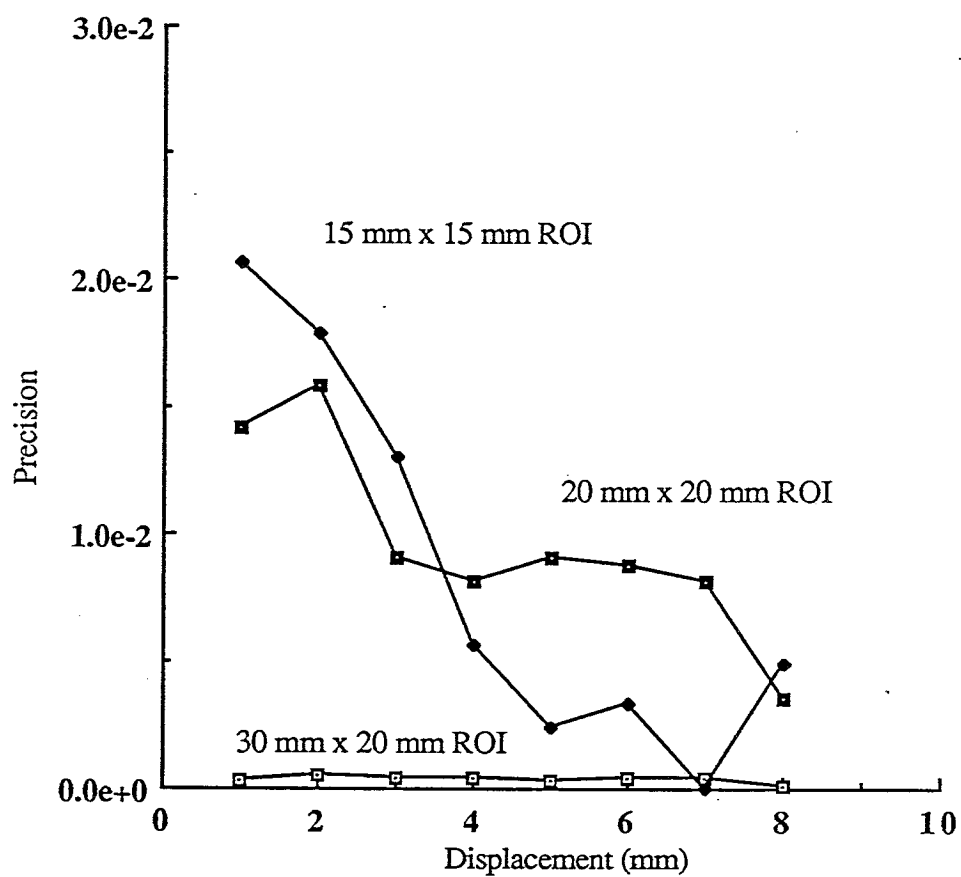


Fig. 10b. Variation of precision with size of region of interest, muscle

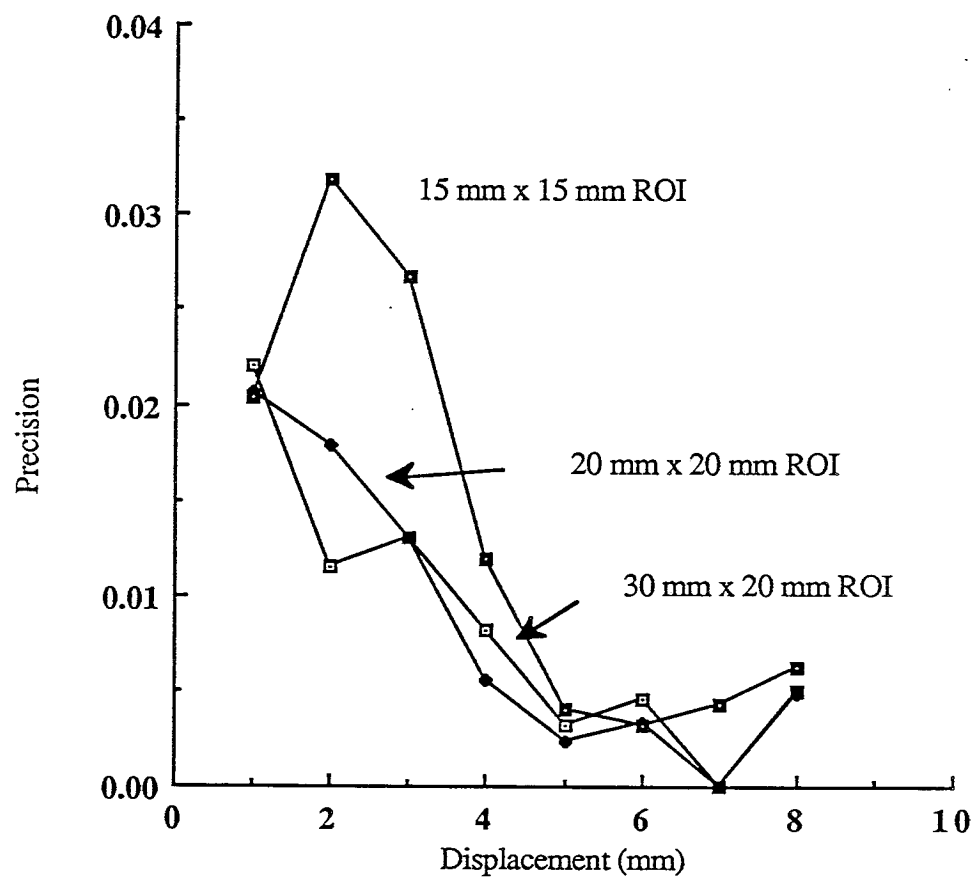


Fig. 10c. Variation of precision with size of region of interest, sponge

5. DISCUSSION

5.1 Interframe Motion of Samples

The problem of estimating the motion of soft tissue structures from two ultrasonic B-scans taken at times t_1 and t_2 was examined. Motion estimates, based on tracking sample motion in intermediate frames, were observed to be significantly better than estimates based on directly correlating noncontiguous frames. It appears that the more intermediate scans (B-scans taken between times t_1 and t_2) that are available, the lower the uncertainty will be in time-domain correlation estimates of sample or structure motion. It appears to be easier to track soft tissue structures over smaller distances and through a larger number of frames than to track them over larger distances and fewer frames. This is a simple and potentially very useful rule of thumb to keep in mind.

5.2 Dependence of Uncertainty on Tissue Type, ROI Size and Actual Sample Displacement

Motion estimates in liver tissue, muscle tissue and sponge produced relative uncertainties in the range of 10% to 20%. Porcine muscle, which contains the greatest internal structure, produced ultrasonic images with the greatest texture and lowest uncertainties. Liver tissue, which is largely homogeneous in structure, produced the greatest uncertainty in motion estimates. There appears to be an inverse relation between the size of a region of interest and the uncertainty in corresponding motion estimates. Based on our limited data it appears that while uncertainties in estimates of tissue motion improve for tissue that exhibit greater structure or texture, they deteriorate for smaller and smaller size ROIs, independent of tissue type. The uncertainty in motion estimates increased linearly at a rate of roughly 0.2 mm per mm, with actual sample displacement for liver tissue, muscle tissue and sponge. This result seems reasonable since motion estimates were based on tracking motion in intermediate frames. This being the case, the motion estimate for a sample displacement $d_2 > d_1$ is partially dependent on the motion estimate for a sample displacement of d_1 and uncertainty in motion estimates cannot and should not ever improve with displacement.

5.3 Dependence of Precision on Tissue Type, ROI Size and Actual Sample Displacement

The time-domain correlation technique produces motion estimates with high precision (less than 1% normalized deviation between estimates for a region of interest with area of at least 100 square centimeters). The exactness of motion estimates using this technique appears to be independent of tissue type. However, the precision of the technique becomes degraded as the size of the region of interest is reduced. This is true for all three sample types.

6. CONCLUSIONS

This thesis has addressed the specific question of how the imperfect correlation between speckle motion and tissue motion affects estimates of tissue displacement, particularly in terms of the uncertainty and precision of such estimates. Quantitative estimates of tissue strain and elasticity, which are based on estimates of tissue displacement, may be limited by uncertainties on the order of 20%. These uncertainties should decrease for tissues that are highly structured and might increase for more homogeneous tissues. It appears that selection of a large region of interest should help reduce uncertainties from estimates of tissue displacement.

Only en-bloc translations of tissue have been considered. That is, no deformations in shape were applied to the ROIs. It would be worthwhile to study the uncertainty in estimates of tissue motion for tissue undergoing graded compressions and external vibrations. Also of interest may be the effect of selecting ROIs containing a border or edge between two different tissue types. Even more exact

results can be obtained with the use of new contrast-detail phantoms [20]. Also of particular interest is the fact that signal processing techniques, applied to M-mode signals, have been developed that may allow for vastly improved depth resolution and measurement of tissue displacements with precision as good as 0.1 mm [21]. It is important to understand the quantitative limitations of estimates of soft tissue motion since calculation of tissue strain and tissue elasticity, which remain important parameters in evaluating mechanical properties of tissue, are largely based on the accurate estimation of tissue displacement.

REFERENCES

- [1] Y. Yamakoshi, J. Sato and T. Sato, "Ultrasonic imaging of internal vibration of soft tissue under forced vibration," *IEEE Transaction on Ultrasonics, Ferroelectrics and Frequency Control*, vol. 32, no. 2, March 1990.
- [2] K. J. Parker, S. R. Huang, R. A. Musulin and R. M. Lerner, "Tissue response to mechanical vibrations for sonoelasticity imaging," *Ultrasound in Medicine & Biology*, no. 3, pp. 241-246, 1990.
- [3] R. M. Lerner, S. R. Huang and K. J. Parker, "Sonoelasticity images derived from ultrasound signals in mechanically vibrated tissues," *Ultrasound in Medicine & Biology*, no. 3, pp. 231-239, 1990.
- [4] M. Tristam, D. C. Barbosa, D. O. Cosgrove, J. C. Bamber and C. R. Hill, "Application of Fourier analysis to clinical study of patterns of tissue movement," *Ultrasound in Medicine & Biology*, vol. 14, pp. 695-707, Feb 1988.
- [5] M. Tristam, D. C. Barbosa, D. O. Cosgrove, J. C. Bamber and C. R. Hill, "Ultrasonic study of in vivo kinetic characteristics of human tissues," *Ultrasound in Medicine & Biology*, vol. 12, pp. 927-937, July 1986.
- [6] J. Ophir, I. Cespedes, H. Ponnekanti, Y. Yazdi and X. Li, "Elastography: A quantitative method for imaging the elasticity of biological tissues," *Ultrasonic Imaging*, vol. 13, pp. 111-134, 1991.
- [7] M. Bertrand, J. Meunier, M. Doucet and G. Ferland, "Ultrasonic biomechanical strain gauge based on speckle tracking," *IEEE Ultrasonics Symposium*, 1989, pp. 859-863.
- [8] R. C. Chivers, "Review Paper: Tissue characterization," *Ultrasound in Medicine & Biology*, vol. 7, pp. 1-20, 1981.
- [9] M. Bertrand, J. Meunier, M. Doucet and G. Ferland, "Ultrasonic Speckle Motion Inherent to Tissue Motion: Theory and Simulation," *IEEE Ultrasonics Symposium*, 1989, pp. 865-868.
- [10] R. Wagner, M. Insana and S. Smith, "Fundamental correlation lengths of coherent speckle in medical ultrasonic images," *IEEE Transactions on Ultrasonics*, Jan 1988.

- [11] Laurence N. Bohs and Gregg E. Trahey, "A novel method for angle independent ultrasonic imaging of blood flow and tissue motion," *IEEE Transactions in Biomedicine and Engineering*, vol. 38, pp. 280-286, Mar. 1991.
- [12] R. J. Dickinson and C. R. Hill, "Measurement of soft tissue motion using correlation between A-scans," *Ultrasound in Medicine & Biology*, vol. 8, pp. 263-271, Sept. 1981.
- [13] I.A. Hein, "Measurement of volumetric blood flow using ultrasonic time domain correlation," Sept 1990, Ph.D. dissertation, University of Illinois, Urbana, IL.
- [14] E. J. Chen, I. A. Hein, R. S. Adler, P. L. Carson and W.D. O'Brien, Jr., "A comparison of the motion tracking of ultrasonic B-mode tissue images with a calibrated phantom," IEEE Ultrasonics Symposium, 1990.
- [15] B. K. P. Horn and B. G. Schunk, "Determining optical flow," *Artificial Intelligence*, vol. 17, pp. 185-203, 1981.
- [16] B. H. Friemel, L. N. Bohs and G. E. Trahey, "A real time system for angle-independent velocity detection," IEEE Ultrasonics Symposium 1990.
- [17] J. T. Chen, "Design and implementation of a high-speed residue number system correlator for ultrasonic time domain blood flow measurement," May 1990, M.S. thesis, University of Illinois, Urbana, IL.
- [18] J. Novakofski, W.D. O'Brien, E. Feleppa and J. Greenleaf, "Applications of ultrasonic technology to major problems in the meat animal industry," Collaborative Research Proposal, National Live Stock and Meat Board, Illinois Beef Council, National Pork Producers, 1990-1992.
- [19] G. E. Mailloux, M. Bertrand and R. Stampfler, "Local histogram information content of ultrasound B-mode echographic texture," *Ultrasound in Medicine and Biology*, vol. 11, no. 5, pp. 743-750, 1985.
- [20] S. Smith, M. Insana and H. Lopeze, "New contrast-detail phantoms for improved precision in lesion detection measurements," *Ultrasound in Medicine & Biology*, vol. 15, no. 4, pp. 383-393, 1989.
- [21] L. S. Wilson and D. E. Robinson, "Ultrasonic measurement of small displacements and deformations of tissue," *Ultrasonic Imaging*, vol. 4, pp. 71-82, 1982.